Electronic Materials Letters (2021) 17:315–323
https://doi.org/10.1007/s13391-021-00291-y

ORIGINAL ARTICLE - ELECTRONICS, MAGNETICS AND PHOTONICS

Electronic Band Transitions in γ-Ge_3N_4

Eduard Feldbach[1] · Andreas Zerr[2] · Luc Museur[3] · Mamoru Kitaura[4] · Geeth Manthilake[5] · Franck Tessier[6] · Veera Krasnenko[1] · Andrei Kanaev[2]

Received: 27 January 2021 / Accepted: 1 April 2021 / Published online: 20 April 2021

Abstract

Electronic band structure in germanium nitride having spinel structure, γ-Ge_3N_4, was examined using two spectroscopic techniques, cathodoluminescence and synchrotron-based photoluminescence. The sample purity was confirmed by x-ray diffraction and Raman analyses. The spectroscopic measurements provided first experimental evidence of a large free exciton binding energy $D_e \approx 0.30$ eV and direct interband transitions in this material. The band gap energy $E_g = 3.65 \pm 0.05$ eV measured with a higher precision was in agreement with that previously obtained via XES/XANES method. The screened hybrid functional Heyd–Scuseria–Ernzerhof (HSE06) calculations of the electronic structure supported the experimental results. Based on the experimental data and theoretical calculations, the limiting efficiency of the excitation conversion to light was estimated and compared with that of w-GaN, which is the basic material of commercial light emitting diodes. The high conversion efficiency, very high hardness and rigidity combined with a thermal stability in air up to ~700 °C reveal the potential of γ-Ge_3N_4 for robust and efficient photonic emitters.

Graphic abstract

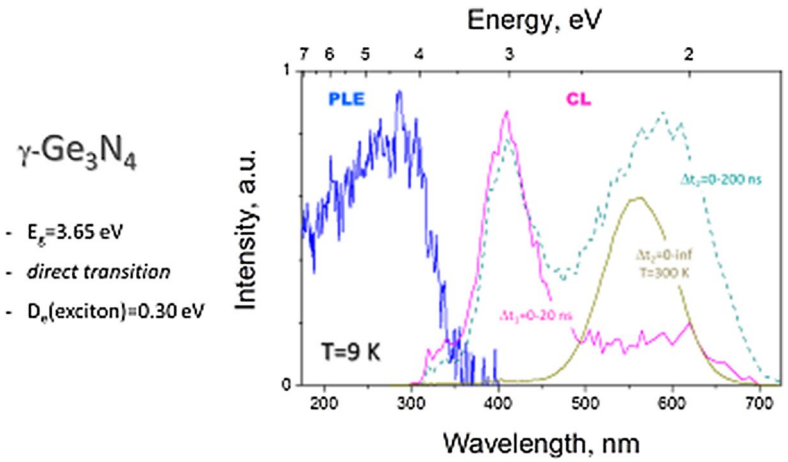

Keywords γ-Ge_3N_4 · Photoluminescence · Cathodoluminescence · Electronic transitions · Exciton

✉ Andrei Kanaev
andrei.kanaev@lspm.cnrs.fr

[1] Institute of Physics, University of Tartu, 1 W. Ostwald str., Tartu, Estonia

[2] Laboratoire des Sciences des Procédés et des Matériaux, CNRS, Université Sorbonne Paris Nord, Villetaneuse, France

[3] Laboratoire de Physique des Lasers, CNRS, Université Sorbonne Paris Nord, Villetaneuse, France

[4] Faculty of Science, Yamagata University, 1-4-12 Kojirakawa, Yamagata 990-8560, Japan

[5] Laboratoire Magmas et Volcans CNRS, IRD, OPGC, Université Clermont Auvergne, 63000 Clermont-Ferrand, France

[6] Institut des Sciences Chimiques de Rennes, CNRS, Université Rennes, Rennes, France

[7] Present Address: Institute of Solid State Physics, University of Latvia, Riga, Latvia

1 Introduction

Germanium(IV) nitride having spinel structure is one of the members of the family of spinel nitrides of the group 14 elements (γ-M_3N_4 where M = Si, Ge, Sn) discovered two decades ago [1–3]. As any high-pressure non-conducting material, γ-Ge_3N_4 exhibits high elastic moduli and hardness [4]; it is also thermally (meta)stable at atmospheric pressure to ~ 700 ºC [5]. More important is that, soon after their discovery, the group 14 spinel nitrides have been predicted to possesses direct band gaps (E_g) spanning the visible wavelength range and extending in the near-IR and UV ranges of light, from 0.6 to 5.0 eV [6–10]. In particular, E_g of γ-Ge_3N_4 was predicted to be between 2.07 and 3.6 eV depending on the applied calculation approach (LDA, GGA, GW etc.). Direct band gap is one of the basic conditions for a material to be considered as an efficient light emitter while a large exciton binding energy ($D_e > > kT$) is the second necessary condition. The latter parameter has been evaluated theoretically by Boyko et al. [7] for all end-members γ-M_3N_4 and their hypothetical solid solutions using the hydrogenic-type model. For γ-Ge_3N_4, the approach led to a large value of $D_e = 174$ meV while the highest $D_e = 333$ meV has been predicted for γ-Si_3N_4 and the lowest $D_e = 69$ meV for γ-Sn_3N_4.

The experimental verifications of the theoretical predictions about the direct interband electronic transition, exciton binding energy and band gap energy of these materials remain rather limited. Boyko et al. [6, 7] have used soft x-ray emission and x-ray absorption spectroscopy measurements to obtain the band gap energies E_g of γ-M_3N_4 (M = Si, Ge, Sn) and $(Ge_xSi_{1-x})_3N_4$ in the range of 1.6–5.0 eV with the relatively low precision of ± 0.2 eV. Later on, Museur et al. [11] have conducted studies of the interband and intraband radiative electronic transitions in γ-Si_3N_4 by time- and energy- resolved luminescence method and obtained $E_g = 5.05 \pm 0.05$ eV and a large free exciton binding energy of ~ 0.65 eV, which is almost twice larger compared to that theoretically predicted. Today, these papers exhaust available experimental data on the electronic transitions in the spinel nitrides of the group 14 elements, γ-M_3N_4.

Furthermore, compounds with the spinel structure [12] have attracted an additional interest during last decades because of their expected high tolerance to high doses of the irradiation with energetic particles [13, 14]. The spinel lattice contains a great number of unoccupied voids, so-called intrinsic structural vacancies: 7/8 of available tetrahedral and 1/2 of octahedral cation sites. For this reason, the spinel lattice can accommodate cations displaced from their regular positions and promote their returning without a significant lattice distortion. Compared with ternary oxides with the general formula AB_2O_4 (where A, B are metal cations and O is oxygen anion), the most known example of which is $MgAl_2O_4$, the binary spinel nitrides γ-M_3N_4 have an additional advantage that antisite defects are not possible in their lattices. This peculiarity, combined with a high hardness, thermal stability in air, direct band gap and large D_e make γ-Si_3N_4 and, potentially, other spinel nitrides interesting as robust and efficient photonic emitters in extreme environments.

In this communication, we report on the first investigation of the electronic band transitions in γ-Ge_3N_4 using UV–visible-near-IR time- and energy- resolved spectroscopy. Based on the obtained experimental data and theoretical estimations, we argue about potentially high efficiency of the excitation conversion to light in this material.

2 Methods

The polycrystalline sample of γ-Ge_3N_4 was synthesized in a multi-anvil press following the procedure reported in Ref. [1] with some modifications. The starting hexagonal phase of germanium nitride, β-Ge_3N_4, was prepared via the reaction of GeO_2 under ammonia flow in a tubular furnace at 880 °C during 12 h. The resulting product was annealed under the same conditions for purity purpose and the phase composition was controlled by X-ray diffraction (XRD) to be pure β-Ge_3N_4. Elemental analyses, performed using a Leco TC-600 analyzer, showed a low level of oxygen contamination of ~ 0.3 wt%. No trace of carbon, eventually coming from the synthesis route or from the used vessels, was found. The β-Ge_3N_4 powder was compacted in an iron capsule (wall thickness 50 µm), compressed in a multianvil press to ~ 13 GPa and heated to 1200 °C for 20 min. The 14/8 assembly with a 14 mm edge length Cr_2O_3-doped MgO octahedral pressure medium and 8 mm tungsten carbide anvil truncation was used. The recovered product was an almost completely sintered cylinder of ~ 1.25 mm in diameter and ~ 1.9 mm in height which split perpendicularly to the cylinder axis in discs of 200–300 µm thickness. One of them, from the sample middle, was used in this study.

The recovered high-pressure product was examined with the powder XRD and Raman spectroscopy. The XRD patterns were obtained using a set-up consisting of a microfocus source delivering Mo *Kα* radiation into a spot of less than 200 µm (IµS high Brilliance-Incoatec Microfocus Source Mo ELM33, Incoatec) and an imaging plate detector with online readout system (mar345, marXperts). In order to obtain high-quality XRD diffractograms, two-dimensional patterns were collected in the grazing incidence geometry at the angle of ~ 7° and converted to

the standard diffractograms $I(2\theta)$ using the Fit2D software [15]. This set-up permits detection of contaminating phases and compounds (e.g. GeO_2) in amounts as low as 0.5 vol.%, not accessible using a standard diffractometer. The Raman spectra were measured with a blue solid-state laser emitting at 473 nm. The spectra were collected by a 100xLWD objective with the lateral resolution of 1 µm using Jobin Yvon HR800 spectrometer equipped with a Peltier cooled CCD detector; the spectral resolution of measurements was 1 cm^{-1}.

The cathodoluminescence (CL) spectra of samples mounted on a close-cycle He cryostat were recorded from the periphery part of sample area at T = 5 K using a setup of the Institute of Physics of Tartu University (for details see Ref. [16]). The reason for avoiding central part of the sample (covered in experiments by Pt foil) was a weak oxygen contamination, as it will be explained below. The CL spectra were recorded with H8259 Hamamatsu photon counting head mounted on ARC SpectraPro 2300i monochromator with 300 l/mm 500 nm blaze grating. The excitation was performed with an electron beam of 10 keV and 0.1 µA. The software for time-resolved CL measurements permitted the collection of emission spectra with different time windows delayed by 5 ns to 2 ms after the excitation pulse of 10 ns duration and rise time of ~ 1 ns with maximum repetition rate of 5 kHz. The time resolution (~ 5 ns) of these measurements was limited by Becker&Hickl MSA-300 multiscaler card and photon counting head response.

The photoluminescence (PL) experiments were carried out at the BL3B beamline [17] of the UVSOR facility with synchrotron radiation excitation in the UV–visible spectral range. The samples were mounted on a cold finger of a LHe flow type cryostat maintained during experiments at T = 9 K in the vacuum of ~ 10^{-7} Pa. In order to increase the signal, PL was collected from the total sample area using Spectra Pro 300i monochromator equipped with a CCD detector. The measured photoluminescence excitation (PLE) spectra were corrected on the detector (AXUV100 photodiode) sensitivity and optical line transmission.

The spectroscopic measurements were accompanied by ab initio numerical calculations using the CASTEP module of the Materials Studio program package [18]. In order to provide more accurate result for Kohn–Sham energy levels, the screened hybrid functional of Heyd-Scuseria-Ernzerhof with optimized screening parameters (HSE06) was used in calculations of the electronic properties on a primitive cell of γ-Ge_3N_4, which permits very reasonable band gap energy values for all three spinel nitride structures of Si_3N_4, Ge_3N_4 and Sn_3N_4: the calculated band values of 4.9 eV, 3.73 eV and 1.79 eV were in a very good agreement with experimental data of 5.05 ± 0.05 eV [11], 3.5 ± 0.2 eV [7] and 1.6 ± 0.2 eV [7] for Si_3N_4, Ge_3N_4 and Sn_3N_4, respectively.

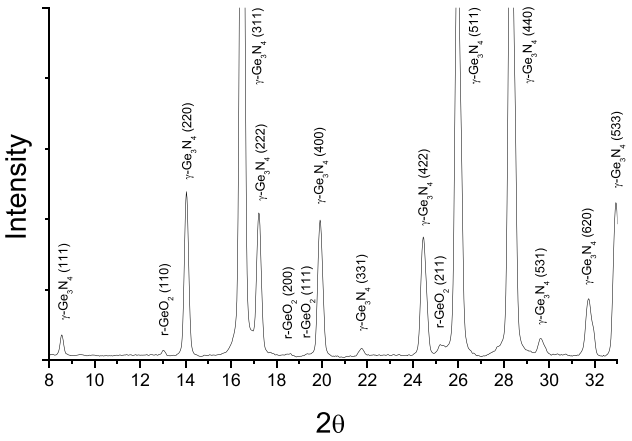

Fig. 1 X-ray diffraction pattern of γ-Ge_3N_4 sample

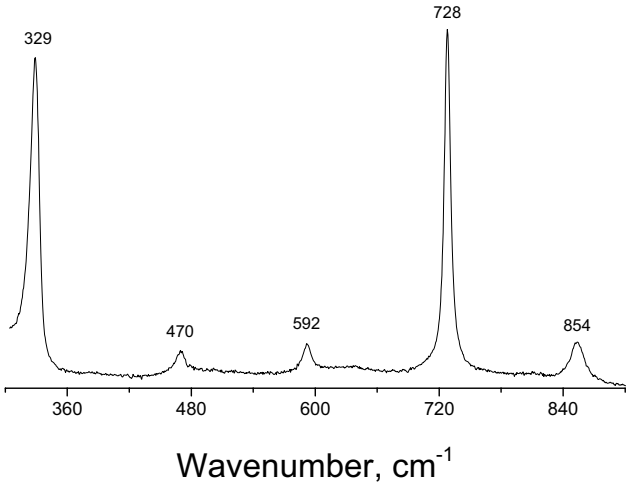

Fig. 2 Raman spectra of γ-Ge_3N_4 sample

The plane-wave basis energy cutoff (with norm conserving pseudopotentials) was chosen to be 700 eV. The Monkhorst–Pack scheme k-points grid sampling was set at 4 × 4 × 4 for the Brillouin zone calculation. The convergence parameters were set as follows: total energy tolerance of 1×10^{-5} eV/atom, maximum force tolerance of 3×10^{-3} eV/nm, maximum stress of 0.05 GPa and maximum atomic displacement of 1×10^{-4} nm. The electronic configurations were $4s^24p^2$ for germanium and $2s^22p^3$ for nitrogen atoms.

3 Results and Discussion

The XRD pattern shown in Fig. 1 indicated an almost pure single phase γ-Ge_3N_4 sample with no admixture of the precursor β-phase. The pattern is dominated by the peaks of **γ**-Ge_3N_4 which positions perfectly agree with the cubic

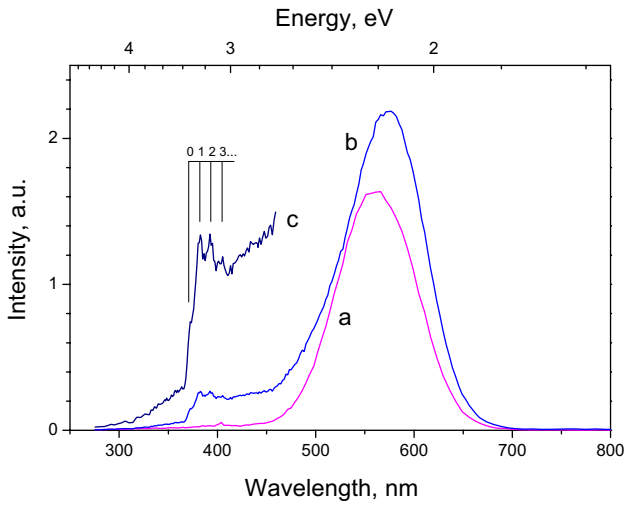

Fig. 3 CL spectra (spectral resolution 1 nm) taken from periphery part of γ-Ge_3N_4 sample at T = 300 K (**a**) and 5 K (**b**, **c**); intensity of (**c**) is that of (**b**) × 5

lattice parameter $a = 8.2125$ Å, reported earlier [19]. Only a very weak oxide phase contamination < 1 vol.% was observed in the central part of the sample attributed to germanium dioxide with rutile structure, r-GeO_2. The periphery regions of the sample were free of any crystalline contamination. Apparently, the iron capsule served as the buffer, which reduced oxygen content in the vicinity of the capsule walls.

The Raman spectra of γ-Ge_3N_4 sample shown in Fig. 2 were dominated by two sharp intense bands at 728 cm^{-1} (T_{2g}) and 329 cm^{-1} (T_g) and three other less intense bands at 854 cm^{-1} (A_g), 592 cm^{-1} (T_{2g}) and 470 cm^{-1} (E_g), which have been previously experimentally observed and theoretically validated to be the five Raman-active modes permitted for the ideal spinel structure [2, 20–22]. No extra high-frequency mode in the range 770–820 cm^{-1} associated with nitrogen vacancies [22] were observed, indicating the expected stoichiometry of the examined sample. The spectra taken in the central and periphery oxygen-free sample parts were identical, confirming a negligible influence of oxidic impurities.

The CL spectra of the γ-Ge_3N_4 sample are shown in Fig. 3. At room temperature, the CL band at 560 nm (2.20 eV) dominated the spectrum. When cooling sample down to 5 K, its spectral maximum red shifted to 575 nm (2.15 eV) and a new UV band appeared as a shoulder at ~ 390 nm, exhibiting a regular structure with the period of ~ 0.09 eV, which corresponds to the strong T_{2g} vibration mode ($\hbar\omega = 90.3$ meV). Such sequence of peaks, well-resolved at low temperatures (5 K in our case), can be attributed to phonon replicas of a zero-phonon line [23], appearing in our CL spectrum at 3.33 eV, as depicted in Fig. 3. This kind of states interpreted as large-radius bound excitons usually appears in solids with Wannier excitons (semiconductors AIIBVI and many others) and has in most cases relatively small binding energy below 100 meV. Because CL spectra were taken from the periphery oxygen-free region of the sample, identification of the defect with the contaminant r-GeO_2 phase can be excluded.

According to our analysis of another member of the high-pressure spinel nitrides, γ-Si_3N_4 [11], two different excited states may contribute to the visible emission: exciton bound to neutral cation X^*-$Si^{\times}$ and metastable paramagnetic anion radical N'^* (in the Kröger-Vink notation). Because of the structural similarity, the both contributions are expected to appear in γ-Ge_3N_4. In order to resolve these two emissions with strongly different excited-state lifetimes, we applied time-resolved CL measurements with short $\Delta t_1 = 0$–20 ns and long $\Delta t_2 = 0$–200 ns time-windows. These measurements were performed with a much lower spectral resolution, which permitted to increase the signal-to-noise ratio (fine vibronic structure of the UV band was not resolved in these spectra). The results shown in Fig. 4 confirmed the expectations: short- and long-lived spectral components were resolved in these measurements. Accordingly, we assigned the spectrum recorded with the long time-window (CL dashed line) with the maximum at λ = 575 nm ($h\nu = 2.15$ eV) to the anion radical N'^*. In contrast, the broad UV emission, which became dominating in the short time-window spectrum (b), has two contributions from (i) non-resolved lines between 3.33 and 3.0 eV due to the large-radius bound exciton and (ii) continuum with spectral maximum at λ = 410 nm (3.0 eV) due to the so-called extrinsic self-trapped or small-radius bound exciton. This

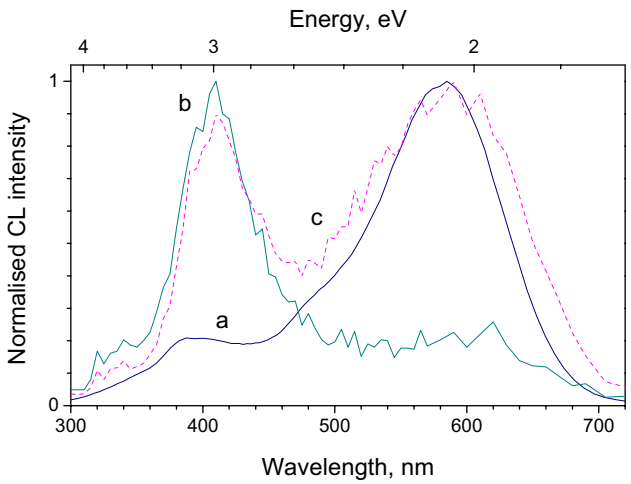

Fig. 4 Integral (**a**) and time-gated (**b**–**c**) CL spectra (spectral resolution 5 nm) taken from periphery part of γ-Ge_3N_4 sample at T = 5 K: $\Delta t_1 = 0$–20 ns (**b**) and $\Delta t_2 = 0$–200 ns (**c**). All intensities are normalized for better visibility

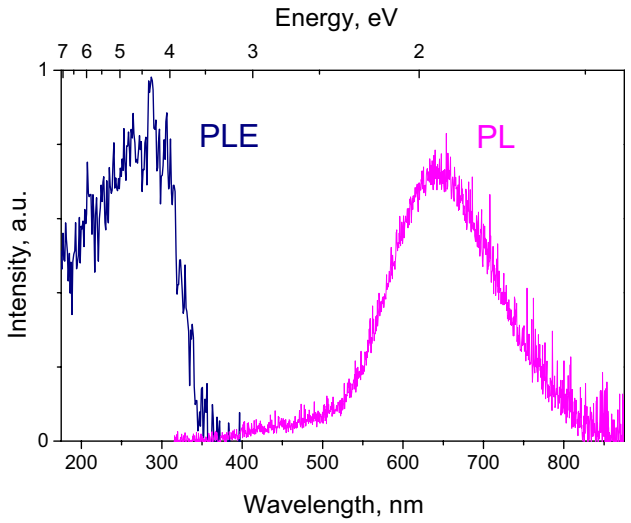

Fig. 5 PL ($E_{exc}=3.95$ eV) and PLE ($E_{PL}=2.05$ eV) spectra of γ-Ge_3N_4 sample at T = 10 K

interpretation is based on the model introduced by Toyozawa [24] and demonstrated experimentally in numerous studies (see e.g. [25–27]). The main point of this model is that in a perfect lattice the strength of the exciton-phonon interaction is not strong enough for the self-trapping of an exciton and the deformation potential of a defect is also not sufficient for the exciton trapping, but the total short range interaction of an exciton with defect and phonons triggers the trapping process. As a result, large- and small-radius bound excitons coexist. Usually defects responsible for this kind of situation are of neutral type, which in our case is, most probably, neutral structural vacancies $V_{Ge}^{\times}$ [28]. The zero-phonon line of the localized exciton X^{*}-$V_{Ge}^{\times}$ was observed at 3.33 eV in the spectrally resolved CL (Fig. 3).

In contrast to CL, PL is state-selective in excitation and can provide more information about the energetic structure. The PL and PLE spectra of γ-Ge_3N_4 sample are shown in Fig. 5. The PL spectrum consists of a broad visible band and a short-wave shoulder at ~400 nm. The apparent red shift of the principal visible PL band with respect to that observed in CL spectra (Fig. 3b) could be, at least partially, explained by sensitivity of H8259 photomultiplier used in CL measurements, which strongly drops at λ > 600 nm. Similarly, a stronger sensitivity of the photomultiplier used in CL measurements with respect to that of the CCD detector of PL setup explains a stronger intensity of the self-trapped exciton in CL spectra (Figs. 4 and 5). By analogy with γ-Si_3N_4 [11], we assume two major contributions of the exciton trapped near neutral cation defect X^{*}-$Ge^{\times}$ and anion radical $N^{'*}$ to the visible PL.

We notice that examination of state-selective PLE spectra for the interband transitions analysis can be preferable in comparison with that of absorbance spectra, because PLE can be free of non-radiative and not relevant (spectrally filtered) radiative transitions of defect/impurity as well as of a contribution of light scattering on grain boundaries in polycrystalline samples. The data examination was performed in agreement with our recent study of γ-Si_3N_4 [11], where visible PL excitation has been shown to fit the interband absorption. We used the Tauc expression for interband transitions in the examined material

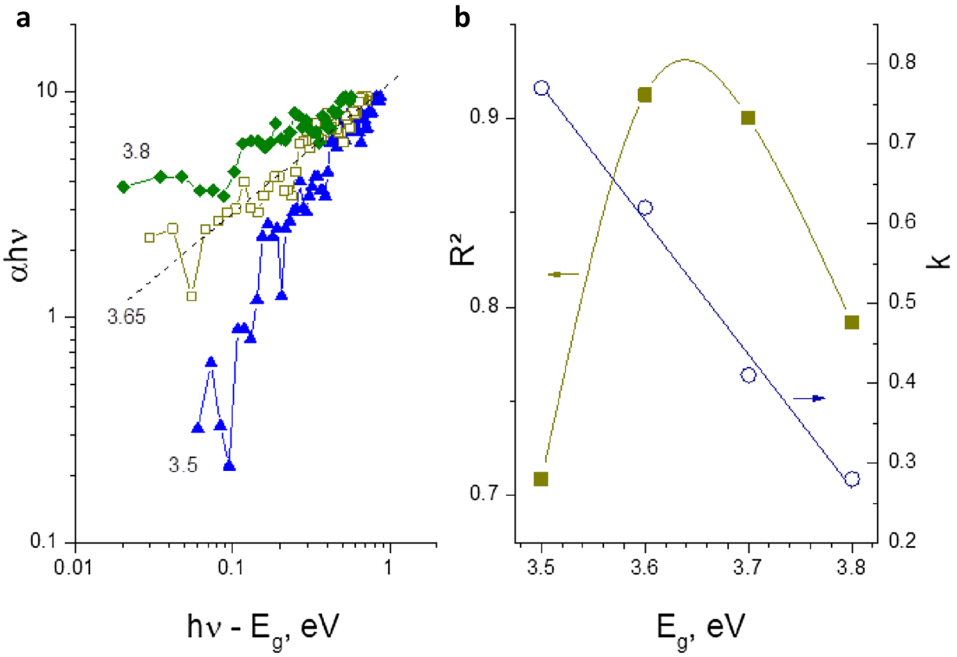

Fig. 6 Modified Tauc plot, according to Eq. (1), obtained from PLE data for several indicated E_g values (**a**) and R^2 and k values derived from the least-squares fits of experimental data in the range of E_g between 3.5 and 3.8 eV (**b**). The adopted solution $E_g=3.65\pm0.05$ eV and k = 1/2 corresponds to the maximum of R^2 (**b**). Solid lines in (**b**) are to guide the eye

$$\lg(\alpha h\nu) = k\lg(h\nu - E_g) + A \quad (1)$$

where α is absorption coefficient, hν and E_g are photon and band gap energies and A and k are constants. The constant k defines the type of the interband transitions: it is equal to 1/2 and 2 respectively for direct and indirect allowed transitions. In the vicinity of the fundamental absorption onset energy, the normalized PLE intensity $I(h\nu)/I_0$ (where I_0 is the maximal PLE intensity) is proportional to the absorption coefficient α. According to Eq. 1, the experimental data in a logarithmic frame should fit a straight line if E_g value is chosen correctly (Fig. 6a); the slope of this line defines constant k and, consequently, type of the interband transitions. More precisely, each of the least-squares fits for a given E_g provided two relevant values of the coefficient of determination R^2 and k, which are plotted as a function of Eg in Fig. 6b. Since the maximum of R^2 defines the best fit by Eq. (1), we adopted $E_g \in [3.6; 3.7]$ eV and k≈1/2 as the best solution in framework of the considered model. Consequently, analysis of the experimental data resulted in the band gap energy $E_g = 3.65 \pm 0.05$ eV and evidenced that the interband transitions of γ-Ge_3N_4 are direct allowed. We note that the earlier reported experimental value of $E_g = 3.5 \pm 0.2$ eV [7] agrees within the experimental uncertainties with the present experimental result.

The obtained experimental data also permitted an important conclusion about the value of the free-exciton binding energy D_e of γ-Ge_3N_4. In fact, a comparison of CL spectra in Fig. 3 indicated the disappearance of the localized exciton (b) at room temperature (a). This signifies that the exciton detached from the weakly bound state with the dissociation energy δE < 25 meV and quenched in the host matrix. Taking into account the position of zero-phonon line at $E^\circ = 3.33$ eV, one can derive the exciton binding energy: $D_e = E_g\text{-}E^\circ\text{-}\delta E \approx 0.30$ eV. We notice that a significantly smaller free exciton binding energy of 174 meV has been calculated for the hydrogen-like exciton [7]. This tendency to the underestimation of the free exciton binding energy has been previously observed for another member of the spinel nitrides family, γ-Si_3N_4, where the experimental value of 0.65 eV [11] was significantly larger than the calculated one of 0.333 eV [7].

The direct allowed transitions in defect-free crystals generally show up in an intense luminescence. We evaluated quantum efficiency of γ-Ge_3N_4 luminescence by a comparison with the reference sample $(Lu,Y)_2Si_5$:Ce (LYSO), which is a well-known efficient scintillator. The comparison showed that the intensity of our sample was about two orders of magnitude lower than that of the reference material. The quantum efficiency of ~0.4% was estimated in our γ-Ge_3N_4. This rather low emission efficiency is characteristic of a non-perfect solid, which is what our polycrystalline sample has to be. Summing up, the synthesis procedure has to be further improved in order to obtain efficient photonic emitters of this material.

The results of the evaluation of the electronic band structure and density of states in γ-Ge_3N_4 using HSE06 calculations with optimized screening parameters [29] are shown in Fig. 7.

Firstly, our calculations confirmed the direct allowed character of the interband transitions in γ-Ge_3N_4. Secondly, the calculated bandgap value of $E_g = 3.73$ eV is in a good agreement with our experimental value of $E_g = 3.65 \pm 0.05$ eV, which is the most accurate one reported so far for γ-Ge_3N_4. According to these calculations, Ge_3N_4 has the direct gap with minimum of the conduction band and maximum of the valence band at Γ point of the Brillouin zone center, as zoom image in Fig. 8a shows. The similar result for γ-Ge_3N_4 has been reported by Gao et al. ($E_g = 3.46$ eV) [30], though Jayatunga et al. [31] have found that the band gap is indirect ($E_g = 3.48$ eV). These both cited authors have used an accurate but very time-consuming GW method of calculations.

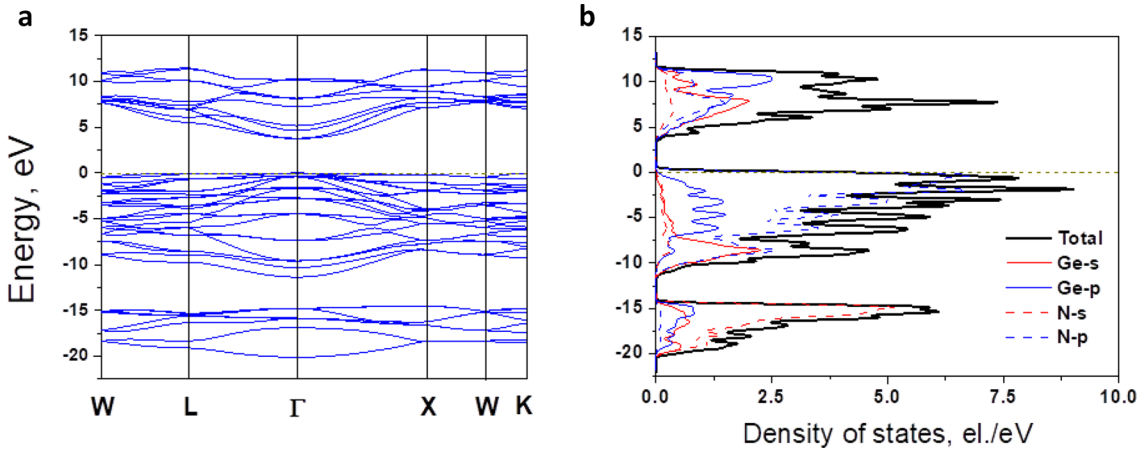

Fig. 7 Electronic band structure (**a**) and density of states (**b**) of γ-Ge_3N_4 obtained from DFT calculations using the HSE06 functional

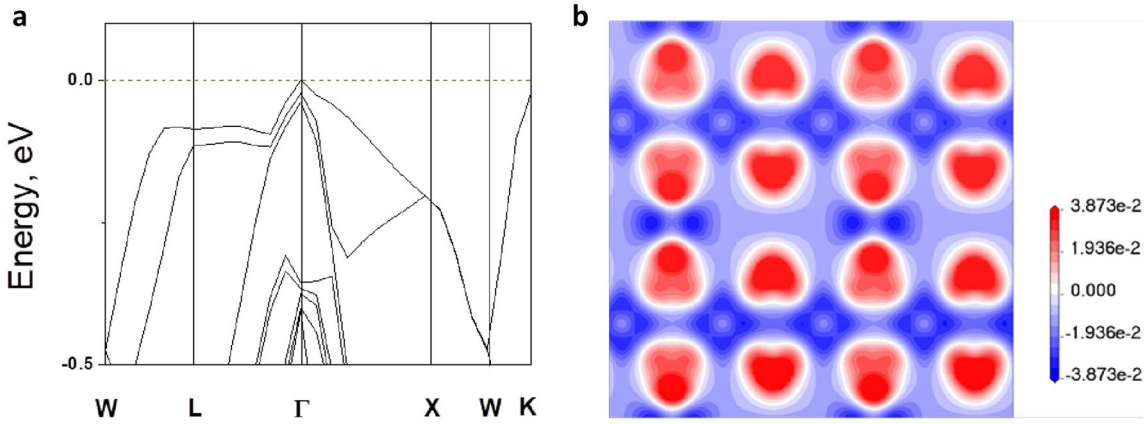

Fig. 8 Magnified/zoomed representation of the top of the valence band of γ-Ge_3N_4 confirming direct nature of band gap (**a**) and charge density difference in cross-section oriented along (0, $\sqrt{2}/2$, $\sqrt{2}/2$) direction and half bond shifted (in electrons/Å^3) (**b**)

Table 1 Effective Mulliken charges of γ-Ge_3N_4 (in units of proton charge)

Species	Electron configuration		Charge (e)
	s	p	
N	1.69	4.49	−1.18
Ge (octahedral)	0.83	1.60	1.57
Ge(tetrahedral	0.86	1.55	1.59

The obtained in the present work effective masses of electron $m_e = 0.58m_0$ and hole $m_h = 5.90m_0$ (m_0 is the mass of free electron) and dielectric constant $\varepsilon = 2.88$ were used in estimations of the emission efficiency (see below). The calculated density of states (DOS) diagram (Fig. 7b) helps to understand the origin of the electronic bands. The valence band in the range from -11 to 0 eV is composed mainly of N 2p states and in the range from −15 to 20 eV of N 2 s states, with a small Ge 4 s and Ge 4p contributions. The contours of the Ge 4p and N 2p curves in the valence band below the Fermi level are similar and overlap indicating the covalent character of the bonds formed between Ge and N atoms. This meets the conclusions by Liu et al. [32]. The conduction band with the width of about 8 eV is formed mainly by a superposition of Ge-p, Ge–s and N-p states; the upper part of the conduction band shows an increasing weight of the Ge-p states.

Our calculations showed that most of the valence electrons are localized on nitrogen atoms. Figure 8b shows the charge density difference in a plane with normal along (0, $\sqrt{2}/2$, $\sqrt{2}/2$) direction of the crystalline lattice and half bond shifted from the atomic plane. This density difference is affected by nitrogen and germanium atoms on the octahedral and tetrahedral sites: Ge-N bond between N-p and Ge-p in the tetrahedral site is slightly more covalent than between N-p and Ge-p in the octahedral site, since it exhibits more elongated shape. The results confirm formation of weak covalent bonds between Ge and N atoms in this structure (see also [32]).

The calculated Mulliken charges [33] for γ-Ge_3N_4 compound are collected in Table 1. We notice slightly different charges of Ge cations in the octahedral and tetrahedral sites.

The results obtained here and published earlier permitted an estimation of the limiting efficiency η of the exciton energy conversion to luminescence in an ideal defect-free crystal, which can be expressed as:

$$\eta = \frac{r_r}{r_r + r_d} \tag{2}$$

where $r_r = 1/\tau_r$ is the rate of exciton radiative transitions (τ_r is the exciton radiative lifetime) and r_d is the exciton dissociation rate estimated from the Onsager-Braun model [34]

$$r_d = \nu \cdot \exp(-D_e/kT) \tag{3}$$

with the frequency factor

$$\nu = 3e(\mu_e + \mu_h)/4\pi\varepsilon a^3 \tag{4}$$

where e, μ_e, μ_h, ε, and a are, respectively, electron charge, electron mobility, hole mobility, dielectric constant and the exciton Bohr radius. In the following, we used our experimental value $D_e \approx 300$ meV for the free-exciton binding energy in γ-Ge_3N_4. Because the physical parameters in Eq. (4) are not measured for γ-Ge_3N_4, we used effective masses of electron from our calculations and estimated the exciton Bohr radius $a = 0.29$ nm. Due to the absence of any experimental or theoretical data on the charge carrier mobility in γ-Ge_3N_4, we used the electron mobility $\mu_e \approx 1$ cm^2/V/s measured in γ-Sn_3N_4 [35], which we consider as representative for the spinel nitrides. We also neglected μ_h in Eq. (4) due to the large effective hole mass. As a result, the

frequency factor $\nu = 4.9 \bullet 10^{14}$ s^{-1} was obtained from Eq. (4) for γ-Ge_3N_4 and Eq. (3) led to the exciton dissociation rate $r_d = 3.0 \cdot 10^9$ s^{-1} at room temperature ($kT = 25$ meV). Taking the radiative free-exciton lifetime $\tau_r \leq 10$ ns, as estimated from our time-gated CL experiments (Fig. 4), we obtained for γ-Ge_3N_4 the exciton emission factor $\eta \geq 3.2\%$ at room temperature. For a comparison, we calculated efficiency η for gallium nitride having wurtzite structure, w-GaN, which is the basic material of commercial light emitting diodes (LEDs). This direct band semiconductor emits in the UVA spectral range ($\lambda \approx 360$ nm) and has a comparable band gap energy ($E_g \approx 3.47$ eV at 0 K) but significantly lower exciton binding energy of $D_e = 26$ meV [36]. We used the following experimental parameters measured at 300 K: dielectric constant $\varepsilon = 5.35$, the effective masses of electrons and holes of $m_e = 0.2m_0$ and $m_h = 0.8m_0$, respectively [37]. Applying the exciton Bohr radius $a = 3.29$ nm [38] and the mobilities $\mu_e = 1000$ $cm^2/V/s$ and $\mu_h \leq 200$ $cm^2/V/s$ [37], we obtained for w-GaN, at room temperature, $\nu = 2.2 \bullet 10^{14}$ s^{-1} and the exciton dissociation rate of $r_d = 7.6 \cdot 10^{13}$ s^{-1}. Accordingly, the exciton emission factor of w-GaN at room temperature was found to be $\eta \approx 0.004\%$ if the free-exciton radiative lifetime $\tau_r = 295$ ps is adopted [39]. Summing up, significantly higher conversion efficiency of the excitation to light could be expected in LEDs based on γ-Ge_3N_4.

The above estimations have shown that high exciton-emission efficiency can be expected in γ-Ge_3N_4, which contains sufficiently low defect concentration. The low luminescence quantum efficiency of ~ 0.4% measured in our polycrystalline sample is characteristic of a strongly non-perfect solid, which is not surprizing on this stage of the research. Accordingly, further efforts are needed to improve the synthesis procedure in order to meet requirements for an efficient photonic emitter based on γ-Ge_3N_4. Furthermore, the earlier and recent reports on a reproducible deposition of γ-Sn_3N_4 [35, 40, 41] show a promising method for large-scale synthesis of the spinel nitrides including thin films of γ-Ge_3N_4.

4 Conclusions

In this work, spectroscopic examination of the electronic interband transitions in γ-Ge_3N_4, synthesized at high pressures and temperatures in a multianvil press, was performed using cathodoluminescence and synchrotron based photoluminescence spectroscopy. The observed luminescence was assigned to (i) coexisting large-radius ($\delta E \leq 25$ meV, $E^{\circ} = 3.33$ eV) and small-radius bound ($h\nu_{max} = 3.0$ eV) excitons trapped near neutral cation defect $V_{Ge}^{\times}$ and (ii) anion radical $N^{'*}$ ($h\nu = 2.15$ eV). The time-gated CL measurements conducted at cryogenic and room temperatures allowed first experimental estimation of the free exciton binding energy: $D_e \approx 0.30$ eV, which suggests exciton stability at room and elevated temperatures. The measurements provided an evidence of the direct allowed interband transitions in γ-Ge_3N_4, which bandgap energy $E_g = 3.65 \pm 0.05$ eV was measured with a higher precision compared to that previously obtained in XES/XANES experiments. The screened hybrid functional Heyd-Scuseria-Ernzerhof (HSE06) calculations with optimized screening parameters supported the experimental conclusions. Based on these results, limiting efficiency of the exciton energy conversion to luminescence in defect-free γ-Ge_3N_4 crystal was estimated and compared with that of w-GaN. The significantly higher conversion efficiency together with advanced mechanical properties reveal the potential of γ-Ge_3N_4 for development of robust photonic emitters, suitable for use in extreme environments.

Acknowledgements This work has been carried out within the framework of the EUROfusion Consortium and has received funding from the Euratom research and training programme 2014-2018 and 2019-2020 under grant agreement No 633053. The views and opinions expressed herein do not necessarily reflect those of the European Commission. Support from Estonian Research Council grant PUT PRG 619 is gratefully acknowledged. The multi-anvil experiments at LMV were supported by the French Government Laboratory of Excellence initiative no ANR-10-LABX-0006, the Région Auvergne and the European Regional Development Fund (ClerVolc Contribution Number 478).

References

1. Leinenweber, K., O'Keeffe, M., Somayazulu, H.H.M., McMillan, P.F., Wolf, G.H.: Synthesis and structure refinement of the spinel, γ-Ge_3N_4. Chem. Eur. J. **5**, 3076–3078 (1991)
2. Serghiou, G., Miehe, G., Tschauner, O., Zerr, A., Boehler, R.: Synthesis of a cubic Ge_3N_4 phase at high pressures and temperatures. J. Chem. Phys. **111**, 4659–4662 (1999)
3. Zerr, A., Riedel, R., Sekine, T., Lowther, J.E., Ching, W.-Y., Tanaka, I.: Recent advances in new hard high-pressure nitrides. Adv. Mater. **18**, 2933–2948 (2006)
4. Shemkunas, M.P., Petuskey, W.T., Chizmeshya, A.V.G., Leinenweber, K., Wolf, G.H.: Hardness, elasticity, and fracture toughness of polycrystalline spinel germanium nitride and tin nitride. J. Mater. Res. **19**, 1392–1399 (2004)
5. He, H., Sekine, T., Kobayashi, T., Kimoto, K.: Phase transformation of germanium nitride (Ge_3N_4) under shock wave compression. J. Appl. Phys. **90**, 4403–4406 (2001)
6. Boyko, T.D., Bailey, E., Moewes, A., McMillan, P.F.: Class of tunable wide band gap semiconductors γ-$(Ge_xSi_{1-x})_3N_4$. Phys. Rev. B **81**, 155207 (2010)
7. Boyko, T.D., Hunt, A., Zerr, A., Moewes, A.: Electronic structure of spinel-type nitride compounds Si_3N_4, Ge_3N_4, and Sn_3N_4 with tuneable band gaps: application to light emitting diodes. Phys. Rev. Lett. **111**, 097402 (2013)
8. Ching, W.Y., Mo, S.D., Ouyang, L., Rulis, P., Tanaka, I., Yoshiya, M.: Theoretical prediction of the structure and properties of cubic spinel nitrides. J. Am. Ceram. Soc. **85**, 75–80 (2002)
9. Chu, I.-H., Kozhevnikov, A., Schulthess, T.C., Cheng, H.-P.: All-electron GW quasiparticle band structures of group 14 nitride compounds. J. Chem. Phys. **141**, 044709 (2014)

10. Hart, J.N., Allan, N.L., Claeyssens, F.: Ternary silicon germanium nitrides: a class of tunable band gap materials. Phys. Rev. B **84**, 245209 (2011)
11. Museur, L., Zerr, A., Kanaev, A.: Photoluminescence and electronic transitions in cubic silicon nitride. Sci. Rep. **6**, 18523 (2016)
12. Sickafus, K.E., Wills, J.M.: Structure of Spinel. J. Am. Ceram. Soc. **82**, 3279–3292 (1999)
13. Sickafus, K.E., Wills, J.M., Minervini, L., Grimes, R.W., Valdez, J.A., Ishimaru, M., Li, F., McClellan, K.J., Hartmann, T.: Radiation tolerance of complex oxides. Science **289**, 748–751 (2000)
14. Sickafus, K.E., Grimes, R.W., Valdez, J.A., Cleave, A., Tang, M., Ishimaru, M., Corish, S.M., Stanek, C.R., Uberuaga, B.P.: Radiation-induced amorphization resistance and radiation tolerance in structurally related oxides. Nat. Mater. **6**, 217–223 (2007)
15. Hammersley, A.P., Svensson, S.O., Hanfland, M., Fitch, A.N., Hausermann, D.: Two-dimensional detector software: from real detector to idealised image or two-theta scan. High Pressure Res. **14**, 235–248 (1996)
16. Feldbach, E., Tõldsepp, E., Kirm, M., Lushchik, A., Mizohata, K., Räisänen, J.: Radiation resistance diagnostics of wide-gap optical materials. Opt. Mater. **55**, 164–167 (2016)
17. Kitaura, M., Tanaka, S., Itoh, M., Ohnishi, A., Kominami, H., Hara, K.: Excitation process of Ce^{3+} and Eu^{2+} ions doped in $SrGa_2S_4$ crystals under the condition of multiplication of electronic excitations. J. Luminescence **172**, 243–248 (2016)
18. Accelrys Software. Material Studio Release Notes, Release 6.1, San Diego (2012)
19. Leinenweber, K., O'Keeffe, M., Somayazulu, M., Hubert, H., McMillan, P.F., Wolf, G.H.: Synthesis and structure refinement of the spinel, γ-Ge_3N_4. Chem. Eur. J. **5**, 3076–3078 (1999)
20. Deb, S.K., Dong, J., Hubert, H., McMillan, P.F., Sankey, O.F.: The Raman spectra of the hexagonal and cubic (spinel) forms of Ge_3N_4: an experimental and theoretical study. Solid State Commun. **114**, 137–142 (2000)
21. Dong, J., Sankey, O.F., Deb, S.K., Wolf, G., McMillan, P.F.: Theoretical study of b-Ge_3N_4 and its high-pressure spinel g phase. Phys. Rev. B **61**, 11979 (2000)
22. Soignard, E., McMillan, P.F.: Raman spectroscopy of γ-Si_3N_4 and γ-Ge_3N_4 nitride spinel phases formed at high pressure and high temperature: Evidence for defect formation in nitride spinels. Chem. Mater. **16**, 3533–3542 (2004)
23. Museur, L., Feldbach, E., Kanaev, A.: Defect related luminescence of hexagonal boron nitride. Phys. Rev. B **78**, 155204 (2008)
24. Toyozawa, Y.: Electron induced lattice relaxation and defect reactions. Physica **116B**, 7–17 (1983)
25. Fel'dbach, ÉKh., Lushchik, Ch.B., Kuusmann, I.L.: Coexistence of large- and small-radius excitons bound on defects in solids. JETP Lett. **39**, 61–64 (1984)
26. Nakahara, J., Kobayachi, K.: Edge emissions and broad-band emissions in thallous halides. J. Phys. Soc. Jap. **40**, 180–188 (1976)
27. Takahei, K., Kobayashi, K.: Impurity-induced self-trapping of holes and minority-ion percolation in TlCl-TlBr mixed crystals. J. Phys. Soc. Jpn. **44**, 1850–1860 (1978)
28. Feldbach, E., Kudryavtseva, I., Mizohata, K., Prieditis, G., Räisänen, J., Shablonin, E., Lushchik, A.: Optical characteristics of virgin and proton-irradiated ceramics of magnesium aluminate spinel. Opt. Mater. **96**, 109308 (2019)
29. Krukau, A.V., Vydrov, O.A., Izmaylov, A.F., Scuseria, G.E.: Influence of the exchange screening parameter on the performance of screened hybrid functionals. J. Chem. Phys. **125**, 224106 (2006)
30. Gao, S.-P., Xu, G.C.Y.: Band structures for Ge_3N_4 polymorphs studied by DFT-LDA and GWA. Comput. Mater. Sci. **67**, 292–295 (2013)
31. Jayatunga, B.H.D., Lambrecht, W.R.L.: Quasiparticle self-consistent GW energy band calculations for Ge_3N_4 phases. Phys. Rev. B **102**, 195203 (2020)
32. Liu, Z., Liu, Y., Li, D., Wei, S., Wu, G., Tian, F., Bao, K., Duan, D., Yu, H., Liu, B., Cui, T.: Insights into antibonding induced energy density enhancement and exotic electronic properties for germanium nitrides at modest pressures. Inorg. Chem. **57**, 10416–10423 (2018)
33. Mulliken, R.S.: Electronic population analysis on LCAOMO molecular wave functions. J. Chem. Phys. **23**, 1833–1840 (1955)
34. Braun, C.L.: Electric field assisted dissociation of charge transfer states as a mechanism of photocarrier production. J. Chem. Phys. **80**, 4157–4161 (1984)
35. Caskey, C.M., Seabold, J.A., Stevanovic, V., Ma, M., Smith, W.A., Ginley, D.S., Neale, N.R., Richards, R.M., Lany, S., Zakutayev, A.: Semiconducting properties of spinel tin nitride and other IV_3N_4 polymorphs. J. Mater. Chemistry C **3**, 1389–1396 (2015)
36. Viswanath, A.K., Lee, J.I., Kim, D., Lee, C.R., Leem, J.Y.: Exciton-phonon interactions, exciton binding energy, and their importance in the realization of room-temperature semiconductor lasers based on GaN. Phys. Rev. B **58**, 16333–16339 (1998)
37. Bougrov, V., Levinshtein, M.E., Rumyantsev, S.L., Zubrilov, A.: Galium nitride (GaN). In: Levinshtein, M.E., Rumyantsev, S.L., Shur, M.S. (eds.) Properties of advanced semiconductor materials GaN, AlN, InN, BN, SiC, SiGe, pp. 1–30. Wiley, NY (2001)
38. Hanada, T.: Basic properties of ZnO, GaN, and related materials. In: Yao, T., Hong, S.K. (eds.) Oxide and nitride semiconductors, pp. 1–19. Springer, Heidelberg (2009)
39. Bunea, G.E., Herzog, W.D., Ünlü, M.S., Goldberg, B.B., Molnar, R.J.: Time-resolved photoluminescence studies of free and donor-bound exciton in GaN grown by hydride vapor phase epitaxy. Appl. Phys. Lett. **75**, 838–840 (1999)
40. Lima, R.S., Dionisio, P.H., Schreiner, W.H., Achete, C.: Magnetron sputtered tin nitride. Solid State Commun. **79**, 395–398 (1991)
41. Maruyama, T., Morishita, T.: Tin nitride thin films prepared by radio-frequency reactive sputtering. J. Appl. Phys. **77**, 6641–6645 (1995)

Institute of Solid State Physics, University of Latvia as the Center of Excellence has received funding from the European Union's Horizon 2020 Framework Programme H2020-WIDESPREAD-01-2016-2017-TeamingPhase2 under grant agreement No. 739508, project CAMART2.